Computational Materials Science 246 (2025) 113414

Contents lists available at ScienceDirect

Computational Materials Science

journal homepage: www.elsevier.com/locate/commatsci

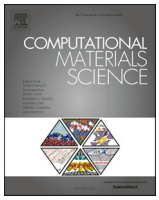

Full Length Article

Influence of non-glide stresses on $\{10\bar{1}2\}$ twin boundary migration in magnesium

Kehang Yu [a], Xin Wang [a,b], Subhash Mahajan [c], Timothy J. Rupert [a,d], Irene J. Beyerlein [e], Penghui Cao [a,d], Julie M. Schoenung [a,f], Enrique J. Lavernia [a,f,*]

[a] Department of Materials Science and Engineering, University of California, Irvine, USA
[b] Department of Metallurgical and Materials Engineering, University of Alabama, USA
[c] Department of Materials Science and Engineering, University of California, Davis, USA
[d] Department of Mechanical and Aerospace Engineering, University of California, Irvine, USA
[e] Mechanical Engineering Department, Materials Department, University of California, Santa Barbara, USA
[f] Department of Materials Science and Engineering, Texas A&M University, College Station, TX, USA

ARTICLE INFO

Keywords:
Twin boundary migration
Twinning disconnection
Nudged elastic band
Energy barrier
Non-glide stress

ABSTRACT

Twin thickening occurs via the migration of a twin boundary during deformation and serves as an important mechanism for accommodating plastic strain. While the local stress state significantly influences twin boundary migration, the precise relationship remains unclear and difficult to determine experimentally. Here, we investigate $\{10\bar{1}2\}$ coherent twin boundary migration in Mg under various stress fields by using the nudged elastic band method to calculate its minimum energy path and hence migration barrier. The results reveal an appreciable influence of non-glide stresses on coherent twin boundary migration. Specifically, the presence of a compressive normal stress reduces the energy barrier. We formulate a phenomenological model to describe the energy barrier as a function of the ratio between the shear stress and the critical resolved shear stress for coherent twin boundary migration. Our results reveal that non-glide stresses can change the critical resolved shear stress and, consequently, the probability of coherent twin boundary migration. In addition, by examining the atomic mechanisms underlying coherent twin boundary migration, we find that the relative atomic displacement at the twinning disconnection observed during coherent twin boundary migration is smaller than the one widely reported in the literature. The energetically favorable configuration of this twinning disconnection varies for different non-glide stresses, causing a non-glide stress-dependent energy barrier. This study advances the understanding of fundamental deformation mechanisms and can contribute to improving models of twinning-induced plasticity.

1. Introduction

The limited strength and low ductility of Mg and Mg-rich alloys are a direct result of their hexagonal close packed (hcp) structure [1]. According to the von Mises criterion, five independent slip systems are needed to accommodate an arbitrary shape change without cracks for a polycrystalline material under plastic deformation [2]. However, for a hexagonal close packed (hcp) structure like Mg, accommodating any deformation requires systems that accommodate both <a> and <c> axis deformation. Mg has four independent slip systems that can be easily activated at room temperature, and both accommodate only <a> -axis deformation, i.e., two independent systems of basal <a> slip and two independent systems of prismatic <a> slip. Consequently, activation of pyramidal <c + a> slip or deformation twinning, in addition to dislocation <a> slip, is needed. Among <c + a> -type mechanisms, $\{10\bar{1}2\}$ deformation twinning is the easily activated one in Mg and in numerous works, has been shown to play a significant role in accommodating plastic strain, often determining material strength and ductility [3,4].

Extension $\{10\bar{1}2\}$ twins develop in multiple stages when deformation is applied, starting with twin embryo nucleation, then propagation of the embryo along the twinning direction into a planar-shaped lamella,

* Corresponding author at: Department of Materials Science and Engineering and J. Mike Walker '66 Department of Mechanical Engineering, Texas A&M University College Station, TX 77840, USA.
E-mail address: lavernia@tamu.edu (E.J. Lavernia).

https://doi.org/10.1016/j.commatsci.2024.113414
Received 27 September 2023; Received in revised form 19 September 2024; Accepted 22 September 2024
Available online 28 September 2024

and finally thickening (growth), during which the lamella expands perpendicular to the twinning plane [5]. Twin thickening involves twin boundary migration, which is generally assisted by nucleation and propagation of twinning disconnections (TDs). TDs are a type of interfacial defect that resides in the twinning plane and is described by a combination of a Burgers vector component, $\boldsymbol{b}$, which is essentially a relative horizontal atomic displacement and will be described as such hereinafter, and a step height component, h [6–8]. TDs are generally mobile and can glide along the twin boundary and shear the crystal, in such a way that the lattice seems to have reoriented the crystal. With the glide of at least one TD, the twin boundary migrates.

It has been shown that the twin boundary is composed of other defects, such as basal-prismatic (BP) interfaces and/or the prismatic-basal (PB) interfaces, which can move and migrate the boundary [9]. Many prior studies of twin boundary migration have involved the interactions between TDs and BP/PB interfaces [10,11] and the sources of TDs [12,13]. Importantly, other studies have been dedicated to understanding the fundamental energetics of mechanisms underlying twin boundary migration. For example, $\{10\bar{1}2\}$ deformation twinning in Mg is dominated by atomic shuffling at room temperature and under normal strain rates, at least during the twin nucleation stage [14]. By studying the energetics of TD gliding in this way, the stable configuration of TDs for each twinning mode can be identified [15]. For instance, it has been shown that a lower energy barrier allows for easier glide of $\{10\bar{1}2\}$ TDs compared to $\{10\bar{1}1\}$ TDs [16]. Through an energetic and structural analysis of the coherent twin boundary (CTB) migration, small activation volume and small critical width of the twinning dislocation dipole have been calculated for $\{10\bar{1}2\}$ twinning transformation, which indicates a feasible twin formation and an adaptive migration behavior of the twin boundary to the local microstructure [17]. A later transition state theory-based study has highlighted the importance of anharmonic vibrational effects and non-glide stresses on the $\{10\bar{1}2\}$ twin boundary migration [18].

Apart from energy, many studies use the applied stress or stress component to modulate the mobility of twin boundaries [5], as well as grain boundaries [19]. A common example concerns the twin resolved shear stress (TRSS), where twin boundary migration is presumed to occur when the TRSS reaches a threshold value, the critical resolved shear stress (CRSS). However, “non-Schmid effects”, or deviations in twinning behavior based only on the TRSS and Schmid factor, have been widely reported [20–26]. Non-Schmid effects are usually explained by stress concentrations or other defects that control behavior [21,22]. However, non-glide stresses which are not accounted for in the TRSS have been explicitly or implicitly excluded in the activation models for twinning [5,27], with only a few studies discussing the role of non-glide stresses on deformation twinning of hcp materials [28–30]. R.A. Lebensohn et al. have found, through an elastic continuum model, the influence of hydrostatic pressure on twin nucleation and propagation is negligible compared to that of the TRSS when they are on the same order [28]. In other studies, C.D. Barrett et al. and K. Ito et al. have showed that non-glide stresses will influence the dislocation core structure before plastic deformation and promote deformation twinning or dislocation glide [29,30]. However, to date there has been no systematic study of the influence of non-glide stresses on deformation twinning.

In this work, we formulate an energetic framework to study the role of non-glide stresses on CTB migration in pure Mg. Using the nudged elastic band (NEB) method, we evaluate the energy barriers, and the results reveal that the compressive stress significantly reduces the barrier for CTB migration. We study the mechanisms underlying this dependence and reveal an important contribution of bulk atom displacement/relaxation that accompanies the glide of TDs. Structural analysis of the intermediate states suggests that the energetically favored TD configuration is subject to change under non-glide stress and may take on a relative atomic displacement at TDs during CTB migration that deviates from its widely reported static value. To enable the prediction of CTB migration under an arbitrary deformation state beyond that simulated, we formulate a phenomenological model to include the non-glide dependence of the energy barrier upon the applied stress field.

2. Methods

To study $\{10\bar{1}2\}$ CTB migration in pure Mg, we use the Large-scale Atomic/Molecular Massively Parallel Simulator (LAMMPS) [31] with a modified embedded atom method potential developed by Wu et al. [32]. This interatomic potential makes robust prediction of $\{10\bar{1}2\}$ twinning behavior because it produces the $\{10\bar{1}2\}$ twin interface and the core structure of the $\{10\bar{1}2\}$ TD, which match first-principles density function theory calculations [32]. Fig. 1(a) shows the simulation cell consisting of a $\{10\bar{1}2\}$ CTB aligned on the xy-plane near the center, with visualization accomplished using OVITO [33]. Hereinafter, the region above the CTB is defined as the twin and that below the CTB as the matrix.

The simulation box of the initial configuration contains 10,880 atoms, and its dimensions are 1.27 nm along the x-direction (i.e., $[\bar{1}2\bar{1}0]$), 15.14 nm along the y-direction (i.e., $[\bar{1}011]$, the twinning direction) and 12.71 nm along the z-direction (i.e., the normal direction to the twinning plane $(10\bar{1}2)$). Periodic boundary conditions (PBCs) are applied along the x- and y-directions, while a non-periodic and shrink-wrapped boundary condition is used in the z-direction. Fig. 1(b) displays the targeted final configuration that has the same type of CTB but after the boundary has migrated two atomic layers with respect to the initial configuration, which is the smallest unit distance of CTB migration. The final configuration is generated by applying shear to the initial configuration followed by a relaxation. Note that the atomic layer between the initial and the final CTB locations is another $\{10\bar{1}2\}$ plane with different x coordinates. Using these initial and final configurations, the NEB method is adopted to study the minimum energy path (MEP) of CTB migration at zero temperature (T = 0 K) [34]. The initial set of intermediate replicas for each NEB calculation is created via a linear interpolation between the defined initial and final configuration. The spring constant for parallel nudging force is 1 eV/Å^2.

For the first set of NEB calculations, a constant normal strain (0 % normal strain, 2 % compressive strain or 2 % tensile strain) is set for each group, while the shear stress is varied in 0.1 GPa increments until the energy barrier reaches zero and CTB migration becomes spontaneous. Similarly, in the other set of calculations, a shear stress (0, 0.3 GPa or 0.6 GPa) is kept constant for each group, while the normal strain is varied by increments of 1 % in the range of −5% to 3 %. The lower tensile strain limit is due to an instability of the NEB algorithm under a large tensile strain. The shear stress τ_{zy} is applied by setting atomic forces to the top and bottom layers, and the normal strain ε_{zz} is applied by imposing a shape change along z to the simulation box. In this study, we investigate the influence of shear stress and normal strain on the activation energy for CTB migration. By manipulating these two independent variables, we can assess how stress affects the process. Specifically, when the defect is isolated at the center of the simulation cell, the local stress at the twin boundary closely matches the atomic stress applied to the top and bottom atomic layers. In this setup, we assume that the applied shear stress represents the TRSS, while the applied normal strain does not contribute to TRSS. Instead, it acts as the non-Schmid component, which is a focal point of our research.

NEB calculations under a pure tensile strain are performed using 32 replicas (i.e., 30 intermediate configurations plus 1 initial configuration and 1 final configuration) and the stress-free case using 46 replicas. All other NEB calculations are performed with 64 replicas. Different numbers of replicas are chosen to attain better convergence for all the NEB calculations described in this paper, and this adjustment does not significantly affect the results. It is important to note that initial and final configurations are relaxed using a conjugate gradient algorithm to

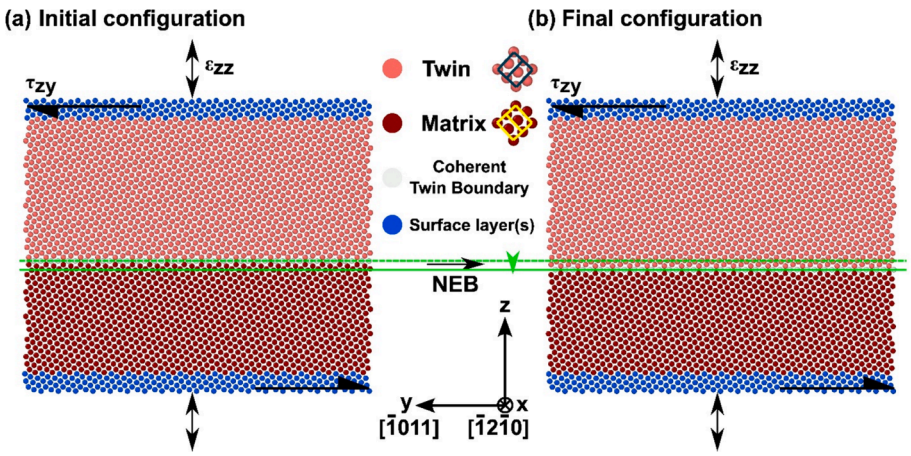

Fig. 1. The snapshots of the initial and final atomic configurations (before and after twin boundary migration) used in the nudged elastic band (NEB) calculations. Atoms are colored based on different regions, i.e., matrix, twin, coherent twin boundary, and surface layers. The coherent twin boundary (CTB) in the final configuration has migrated two atomic layers from its initial configuration. The shear stress τ_{zy} and the normal strain ε_{zz} can be imposed on the system, as indicated.

ensure systems are at a local energy minimum.

3. Stress-dependent migration path and energy barrier

3.1. Stress-dependent minimum energy path (MEP)

Fig. 2(a) shows the normal strain-dependent MEPs of CTB migration under zero applied shear stress. The reaction coordinate represents the progress of CTB migration and is defined as the two-norm of 3 N-length distance vector between the atoms at the current replica and those at the initial replica, where N is the total number of atoms in the system. Note that in the MEPs of this work, the y-axis is labeled as Δ potential energy (i.e., change in potential energy) and that the absolute value of potential energy for these initial configurations under different applied stress is not the same. The energy barrier is defined as the potential energy difference between the maximum potential energy along the MEP and the initial potential energy, as shown in Fig. 2(a).

The MEP under stress-free condition is depicted by the "0% normal strain" curve in Fig. 2(a). The symmetry of the MEP curve also indicates that the stress-free migration event is equally likely to happen also in a reverse way (i.e., CTB migrating upwards by two atomic layers from the final configuration to the initial one). Moreover, the symmetry of the stress-free MEP represents an essential confirmation of the validity of this calculation setup, as the initial and final states under stress-free conditions should retain the same potential energy. The MEP curve gets flattened as the normal strain increases either way, compressive or tensile, while the curve remains nearly symmetric as long as there is no shear stress. The flattening of the migration path and the observed decrease in energy barrier indicate the normal stress dependence of CTB migration. In all the MEPs presented in this work, two special replicas corresponding to TD nucleation and TD recombination are labeled. These two replicas divide the entire migration process into three stages: before TD nucleation, TD gliding, and after TD recombination.

In Fig. 2(b), the MEPs of CTB migration are found to vary with the applied shear stress (i.e., with a zero normal stress). Fig. 2(c) enlarges the highlighted section of Fig. 2(b). As shear stress increases, a potential energy difference between the initial and the final configuration appears. This directly results in a lower energy barrier for CTB migration and a higher energy barrier for the reverse migration. Therefore, CTB migration is heavily biased towards moving along the −z direction of the simulation box. Another important observation is that the downward shift of the central region of the MEP with increasing shear stress, which corresponds to spontaneous TD gliding after the saddle point is reached when TDs nucleate. We did not use free-end NEB for this study. Our calculations did not use the free-end NEB method, meaning the initial and final states were fixed throughout. It is important to note that the initial and final configurations were relaxed to the local energy minimum under the given stress conditions before starting the NEB calculations. After optimizing the MEP in NEB, we enable barrier-climbing to push one of the replicas to the saddle point. Our calculations confirmed that the identified saddle points met the optimized criteria.

In Fig. 2(d), we show MEPs in which the normal strain was varied, while the shear stress was kept constant at 0.6 GPa. Fig. 2(e) enlarges the critical region of the MEPs delineated by a red box in Fig. 2(d). The normal strain, unlike the shear stress, does not result in a significant energy difference between the initial and the final configurations. The compressive strain lowers the energy barrier for TD nucleation, while the tensile strain slightly increases it compared to that without normal strain. The replicas where TDs nucleate have a similar reaction coordinate for all three normal strain levels, while the TD recombination happens later under tensile strain compared to the other two.

3.2. Energy barrier as a function of shear stress and normal strain

This study examines the impact of the stress field on the energy barrier for CTB migration. The data is analyzed from two perspectives, as presented in Fig. 3. Fig. 3(a) shows that the shear stress is varied at three constant normal strain levels. The imposed shear stress reduces the energy barrier for all three normal strain values (−2%, 0 %, 2 %). A potential modification to the model addressing the role of non-glide stresses suggests that the CRSS, at which the energy barrier becomes zero, is not constant but instead depends on the applied normal strain. This contrasts with previous studies that overlooked the influence of non-glide stresses [5,27]. Compressive strain notably reduces the CRSS, significantly facilitating CTB migration, whereas tensile strain slightly increases the CRSS, thereby impeding CTB migration.

Certain crystal plasticity models, though not all, assume a power law relationship between the shear rate ($\dot{\gamma}$) caused by a plastic deformation system and the ratio of the TRSS (τ_r) to the CRSS (τ_c) for that system, as expressed in Eq. (1).

$$\dot{\gamma}^s = \dot{\gamma}_0 \left(\frac{\tau_r^s}{\tau_c^s} \right)^n \tag{1}$$

Here, n represents a constant interpreted as the inverse of strain rate sensitivity for slip, and the superscript s denotes the slip system [34,35]. This power-law relationship is inspired by the constitutive equation used to describe non-linear viscosity [36]. Consequently, even if the TRSS is below the CRSS, the slip system can still contribute to deformation, although to a lesser extent.

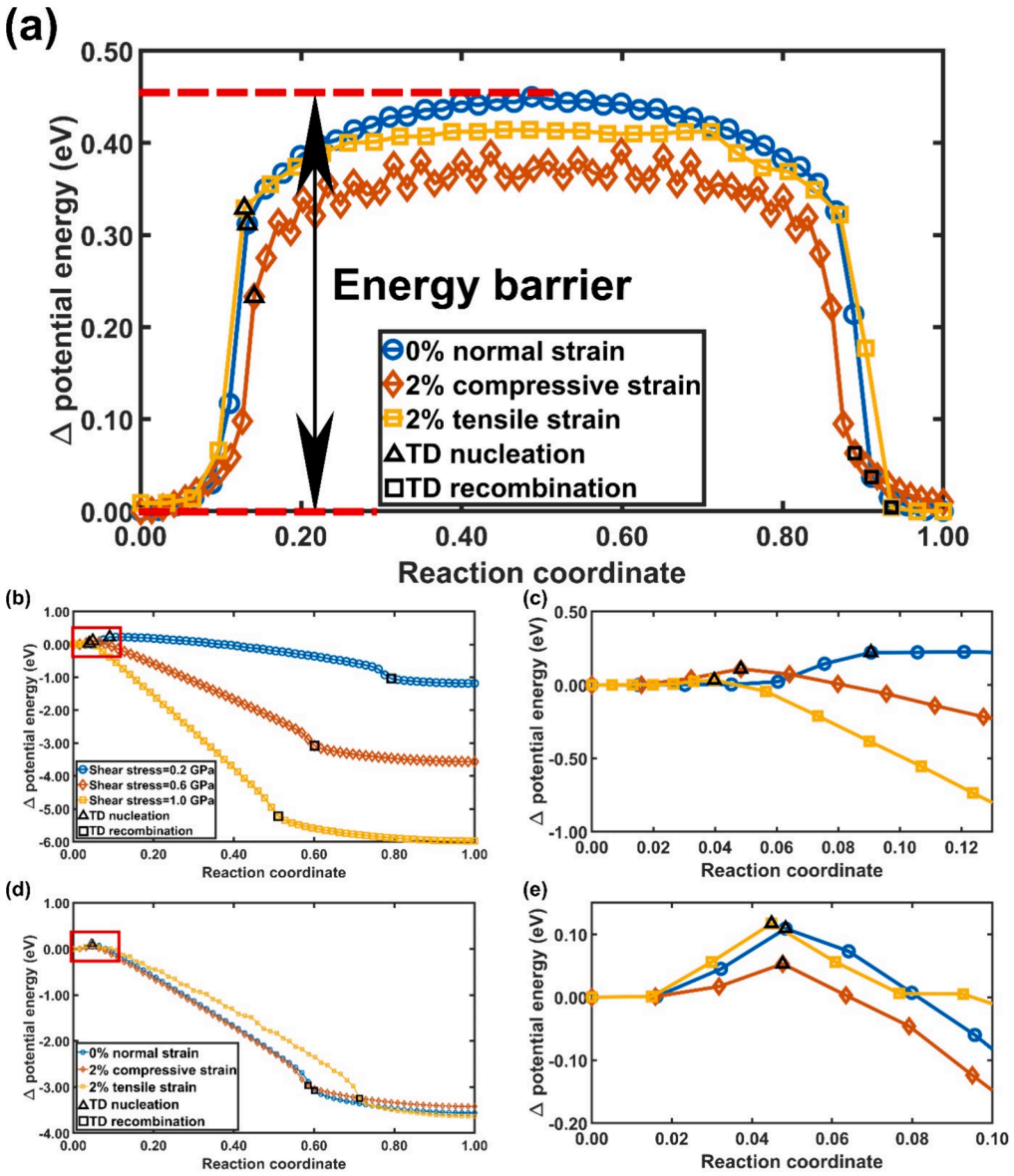

Fig. 2. (a) Normal strain-dependent minimum energy paths (MEPs) under zero applied shear stress as a function of reaction coordinate (RC). The replicas labeled with triangles represent when twinning disconnections (TDs) nucleate and those labeled with squares represent when TDs recombine and cancel each other. The energy barrier in this study is defined as the energy difference between the saddle point and the initial local minimum. (b) Shear stress-dependent MEPs under zero applied normal strain as a function of the reaction coordinate. An enlarged view of a few highlighted starting replicas including the saddle point is provided in (c). (d) Normal strain-dependent MEPs under an applied shear stress of 0.6 GPa as a function of RC. An enlarged view of a few highlighted starting replicas including the saddle point is provided in (e).

It can be shown that this logarithmic function, among a set of elementary functions, best fits the energy barrier-shear stress relationship given by the MEPs. Here in Fig. 3(a), the fitted curves show a relationship in the form of:

$$E_{barrier} = A \cdot \ln\left(\frac{\tau_r}{\tau_c}\right) \tag{2}$$

where τ_r is the TRSS and equal to the applied shear stress since the resolved component of normal loading along y-direction to twin direction (i.e., z-direction) on the twin plane (i.e., xy-plane) is zero and therefore the non-glide stress does not contribute to the TRSS [27], τ_c is the CRSS for CTB migration and is the x intercept of the curve and A is a constant. This relationship suggests that the ratio between the TRSS and the CRSS values correlates with the calculated energy barrier.

For all the shear stress levels above zero in Fig. 3(b), the imposed compressive strain decreases the energy barrier while the tensile strain increases the energy barrier but less significantly. This trend matches the observation in Reference [18]. An exception is observed for 3 % tensile strain under 0.6 GPa shear stress where the energy barrier slightly decreases. The zero energy barriers shown in Fig. 3(b) also indicate that the CRSS is further lowered down to below 0.6 GPa under 4 % compressive strain and to below 0.3 GPa under 5 % compressive strain. Briefly, Fig. 3(a) and 3(b) altogether reveal the significant role the compressive strain may play in assisting CTB migration. Though further investigation is beyond the scope, the non-glide stress dependence should be expected for other twin boundaries (e.g., $\{10\bar{1}1\}$ CTB).

The computational results show the variation in the non-glide stress-induced CRSS and CTB migration barrier. This may provide an explanation to the reported breakdown of the Schmid law from experiments [20,25,29]. To further reveal the shear rate dependency upon the TRSS and the CRSS, we assume we can apply transition state theory, which states that an event's probability can be described with an Arrhenius

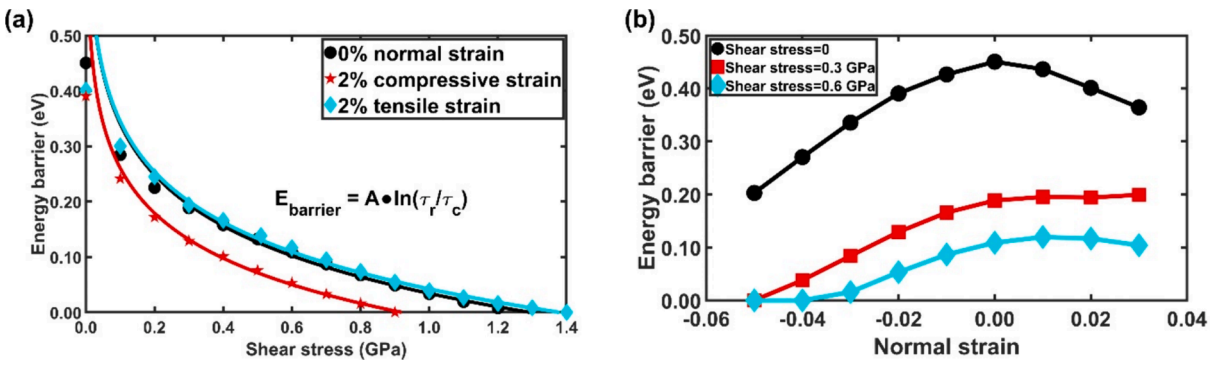

Fig. 3. (a) Energy barrier of coherent twin boundary migration as a function of shear stress under three different normal strain levels (0 % normal strain, 2 % compressive strain and 2 % tensile strain). Fitted curves following the equation $E_{barrier} = A \cdot \ln\left(\frac{\tau_r}{\tau_c}\right)$ are also given, where τ_c is a constant dependent on the imposed normal strain. (b) Energy barrier of CTB migration as a function of normal strain under three different shear stress levels (0, 0.3 GPa, and 0.6 GPa).

equation such as:

$$\dot{\gamma} \propto \exp\left(-\frac{E_{\text{barrier}}}{kT}\right) \tag{3}$$

where $\dot{\gamma}$ here represents the rate of CTB migration, k is Boltzmann constant, and T is the absolute temperature. It is also implicitly assumed that the energy barrier is independent of temperature by using the calculated energy barrier under a non-zero temperature. Combining Eqs. (2) and (3), one can reduce them to the form of Eq. (1), which is:

$$\dot{\gamma} \propto \left(\frac{\tau_r}{\tau_c}\right)^n \tag{4}$$

where n is the same constant in Eq. (1) and equal to $-\frac{A}{kT}$. Table 1 contains the model parameters for three groups of calculations under different normal strains. To keep the problem tractable, we assume n to remain constant, given its smaller variability, and CRSS is varied by the applied non-glide stress, although this assumption should be examined in detail in future work.

This model matches the acquired data from NEB calculations with R-squared values of all three fittings above 0.99. The only discrepancy appears when the shear stress approaches zero. For Eq. (3), mathematically, one will have an energy barrier value approaching infinity if τ_r stays positive but gets closer to 0, which is physically unrealistic. This will not greatly affect the model's migration rate prediction. This is because under a shear stress approaching 0, the CTB migration has nearly the same probability of happening in each direction (i.e., migrating upwards or downwards) and the net migration is thus much less likely to happen. Consequently, $\dot{\gamma}$ in Eq. (4) should, both theoretically and via this model, be at a very low level in the case of $\tau_r \sim$.

Generally, Eq. (4) has the same format as Eq. (1) and the data from NEB calculations can even give a suggested value of the constant in the exponent of the ratio between the TRSS and the CRSS (i.e., n in this study) because NEB analysis correlates the energy barrier and the TRSS. The two scales, the TRSS through the flow rule and the energy barrier through the Arrhenius equation, are consistent in predicting the CTB migration event at this point.

Table 1
Parameters in Eqs. (3) and (4) under different normal strains.

	CRSS (GPa)	A (eV)
0 % normal strain	1.29	−0.133
2 % compressive strain	0.92	−0.117
2 % tensile strain	1.38	−0.131

4. Migration mechanism and mechanistic model

4.1. Migration mechanism

In addition to the energy barrier, the NEB calculations can also reveal the intermediate states along MEPs, providing information on the CTB migration mechanism at the atomic scale. To demonstrate, we first consider the load-free CTB migration case to elucidate the migration mechanism and then introduce a case where the shear stress is applied. Fig. 4(a) includes the MEP curve of the load-free CTB migration. Three stages, separated by the two events (i.e., the TD nucleation and the TD recombination), are labeled. Five states (replicas) denoted with A-E along the MEP in Fig. 4(a) are highlighted and their atomic configurations are shown in Fig. 4(b).

Replica A is the critical state right before the pair of TDs nucleates. The atomic configuration of the initial CTB shows that the twin boundary is flat. In contrast, the other atomic layers have the corrugated structure (i.e., two nearest atoms in the same atomic layer have different z coordinates) as shown by the atomic configuration of the twin boundary (colored in white) in replica A of Fig. 4(b). Atoms near the CTB remain static during stage 1 before TD nucleation, while atoms that are farther away from the CTB (referred to as bulk atoms) move, as shown in Fig. 4(c). Only the y displacement is plotted since it is the dominant component compared to x and z displacements. The twin shear seems to happen in bulk atoms even before and after the boundary migrates. The collective motion of these atoms, which corresponds to a minor rise in the total potential energy of the system, is a prerequisite for TD nucleation and later CTB migration. This finding indicates that the atomic configuration in and near the CTB alone cannot fully describe CTB migration, but that bulk atom displacement is required.

After the prerequisite displacement of bulk atoms, a few atoms near the TD nucleation site in the CTB start to move in replica B. Those atoms show the formation of a pair of TDs by shear (i.e., the collective horizontal displacement) and shuffle (i.e., the relative vertical displacement) of the two atoms. In a CTB, to conserve the TD characteristics $\boldsymbol{b}$ and h, TDs tend to nucleate in pairs. Fig. 4(a) also indicates that the process of TD nucleation consumes much energy though the actual atomic displacement and the corresponding range of reaction coordinate is relatively short.

Theoretically the site where the TD pair nucleates in replica B should be random because every site on the CTB is identical given the coherency of the twin boundary and the PBC along the horizontal direction. However, in this study, nucleation always occurs at the edge of the simulation box, which may be caused by some precision-induced minor variation of the lattice parameter along the CTB. A comparative calculation is also conducted where the CTB atom at the center of the simulation box is displaced by a tiny distance (e.g., 0.001 Å). As shown by

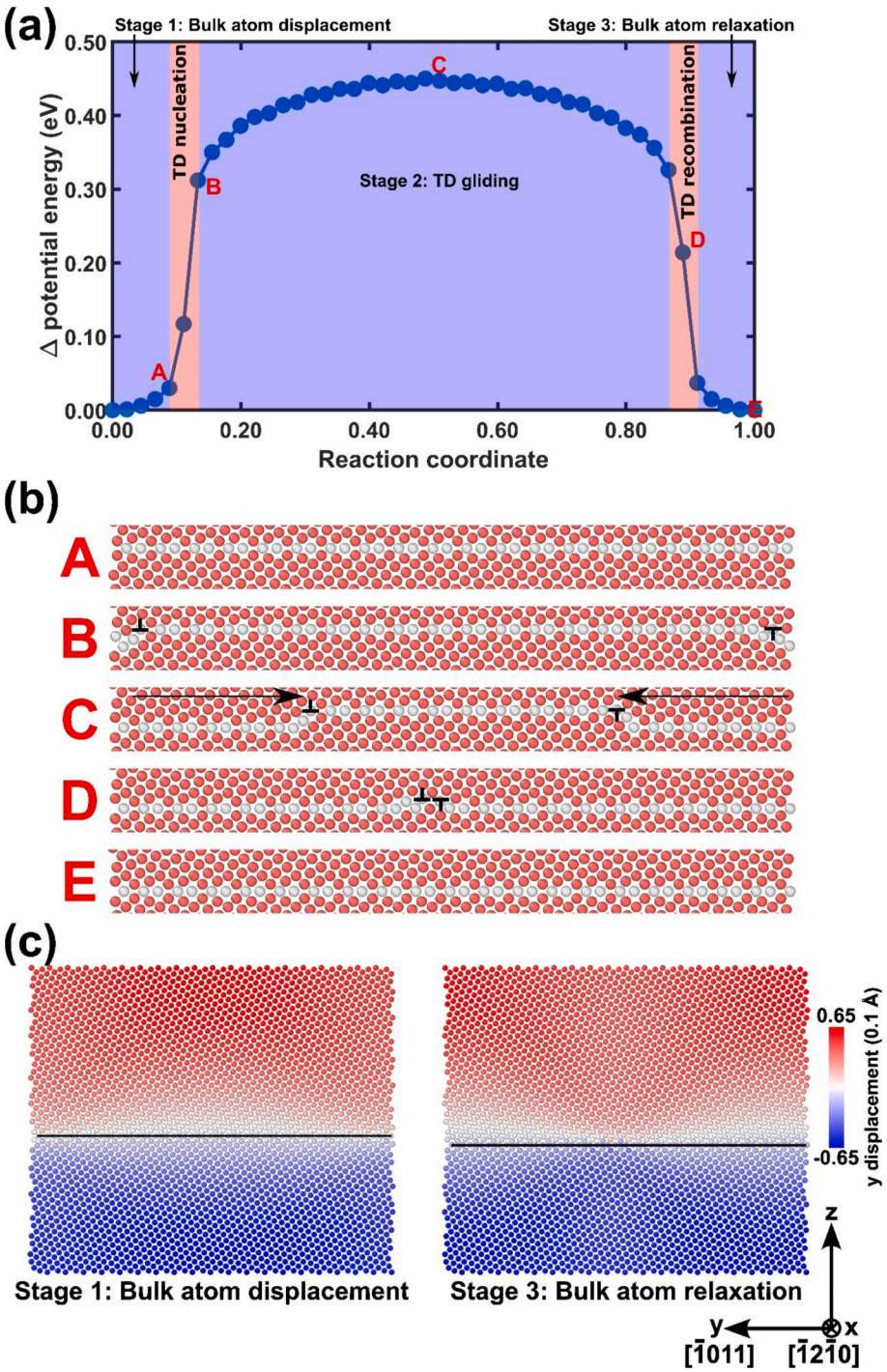

Fig. 4. (a) The minimum energy path (MEP) of the coherent twin boundary migration under the stress-free condition. Stage 1 (bulk atom displacement), TD nucleation, Stage 2 (twinning disconnection (TD) gliding), TD recombination and Stage 3 (bulk atom relaxation) are colored along the MEP. Five representative states (replicas) A-E are labeled, and their atomic configurations are presented in (b). Atoms are colored based on their local structural environment, red: hcp, gray: boundary atoms that are not of any specified crystal structure type. (c) The atomic displacement during Stage 1 and Stage 3 along the y direction.

Fig. 5, nucleation occurs at the site where the boundary atom is displaced in the CTB instead of the edge, while the MEP and the energy barrier value do not significantly change. Consequently, we do not anticipate that the exact location of the nucleation site will significantly alter the results.

To complete the boundary migration, each TD must propagate in opposite directions on the CTB. Replica C is chosen within stage 2, TD gliding. As the TD pair sweeps through, part of the crystal is reoriented with the final CTB growing. This process also turns the atomic layer of original CTB to be corrugated as other non-CTB atomic layers. Only one representative atomic configuration on the process of TD gliding is shown in Fig. 4(b) since the atomic configuration near all TDs is the same. Energetically, this process also sees a slight potential energy increase to the saddle point in the middle of the MEP followed by a symmetrical potential energy drop. Physically, the symmetry is due to the similarity in both structure and energy of the initial and the final configuration. The saddle point is in the middle because the interaction energy increases as the two TDs depart from each other and then

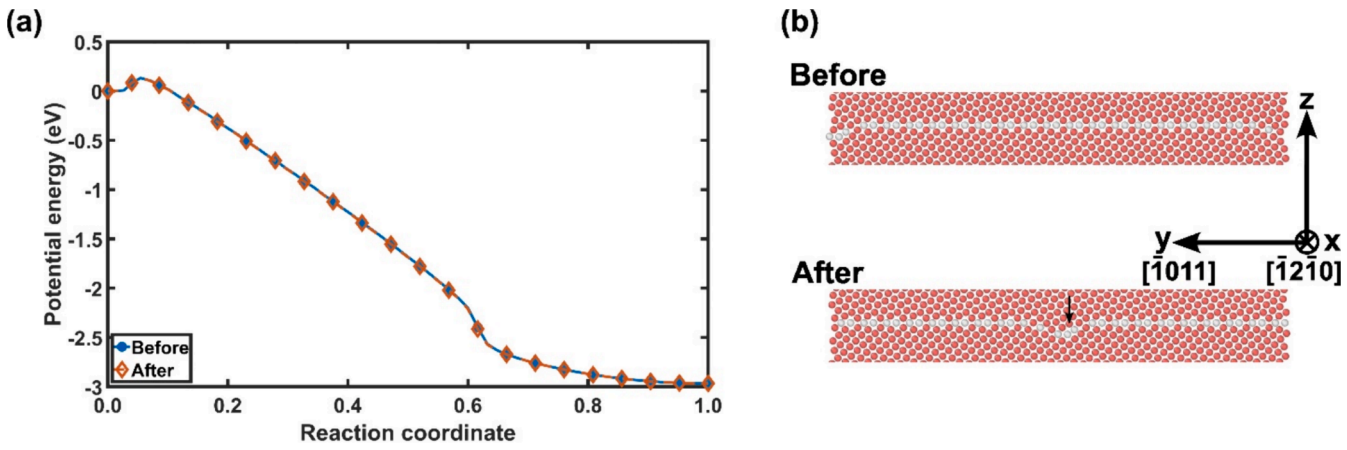

Fig. 5. (a) The minimum energy path of the coherent twin boundary (CTB) migration under a shear stress of 0.5 GPa before and after the + 0.001 Å y-displacement of an atom in the middle of the initial CTB. (b) The atomic configuration of the replicas where the twinning disconnections nucleate before and after the tiny displacement.

decrease again as they get closer again [8].

At the end of the travel of the TD pair, one TD would finally meet the other somewhere in the CTB. Replica D sees the recombination of TDs. Like in TD nucleation, the potential energy drops dramatically due to the restoring of the CTB structure. Moving forward, replica E marks the end of CTB migration. It is observed that bulk atoms, again, displace themselves to further relax the energy of the system and complete the twin shear, as shown in Fig. 4(c).

Based on the above mechanism, there are two key events during the CTB migration process, the nucleation of a pair of TDs and the recombination of them. The former one marks the beginning of TD gliding along the twinning direction, and the latter sees its end where the pair of TDs meets and must recombine and restore the coherency of the twin boundary.

As highlighted in the MEPs of Fig. 2(a), 2(b) and 2(d), all CTB migration processes under different applied stress will go through the processes of bulk atom displacement, TD nucleation, TD gliding, TD recombination, and bulk atom relaxation. The similar migration mechanism also explains why the MEPs shown in Fig. 2 share some common features including: (1) a steeper potential energy rise/fall at the replicas where TDs nucleate/recombine, and (2) a smooth potential energy change during the two stages of bulk atom displacement and relaxation. However, there are still a few noticeable stress-induced variations to the energy pathway. Fig. 6 shows another example of CTB migration, but under a shear stress of 0.5 GPa. While all these processes still exist, both TD nucleation and TD recombination shift to an earlier stage of the MEP under a larger shear stress because of a smaller energy barrier and shear stress-induced broken symmetry of the initial and the final configurations. Also, for all cases with a reasonably high shear stress (precisely, equal to or larger than 0.3 GPa), the energy barrier sits at the exact replica where a pair of TDs nucleates, which means the TD gliding may not consume energy and become spontaneous, as shown in Fig. 6(a). Here, the applied stress field, instead of the TD interaction, significantly changes the energy barrier and the MEP, different from the stress-free case. Fig. 6(b) shows the similarity of atomic configurations near the twin boundary. Fig. 6(c) indicates that another feature, the bulk atom displacement/relaxation before TD nucleation and after TD recombination still occurs, but with a shorter displacement especially before TD nucleation. There is also no other type of disconnections but only a stress-induced configuration variation observed. To understand how the stress field makes a difference to the MEP, we need to examine the structural variations in the TDs.

4.2. Structural variation of the CTB and the TDs upon applied load

The stress-dependent energy barrier difference can be ultimately attributed to the structural variation of the atomic configurations of both the CTB and the TDs upon the stress field. Before discussing the structural variation of the CTB, the atom numbering and the TD labeling are defined in Fig. 7(a) for clarity. Fig. 7(b) illustrates the kite-shaped structural unit in the vicinity of both the initial and the final CTB, which displays the structural variation through this structural unit. Fig. 7(c) and 7(d) both depict two neighboring structural units captured from the initial configuration. For Fig. 7(c), it shows how the structural unit would vary when the applied shear stress increases from 0 to 1.2 GPa – as the shear stress goes up, the structural unit shears accordingly, while the distance between the two neighboring units remains unchanged. In this way, the lattice symmetry about the CTB is broken, which is the structural reason why the MEP will not be symmetrical about the saddle point and CTB migration downwards is energetically favorable. Fig. 7(d) presents the difference of the structural unit upon different applied normal strains. As the normal strain goes from 5 % compressive to 3 % tensile, there is no net shear of the structural unit, and the symmetry of the CTB is kept, which is consistent with the symmetry of MEPs of the normal strain cases. The notable difference here is the stretch along z-direction and some accompanying horizontal displacements as indicated in Fig. 7(d). To understand the structural variation in a quantitative manner, Fig. 7(e) defines the relative horizontal displacement for atoms in the initial CTB by comparing the atom position with the imaginary atom belonging to the lattice below the initial CTB.

Fig. 7(f) and 7(g) show the necessary relative horizontal displacement normalized by the length of $[10\bar{1}1]$ for atoms in the initial CTB, denoted as ultimate α, to move to their positions in the final configuration. This value should be equal to the magnitude of the Burgers vector of a full TD upon stress normalized by $[10\bar{1}1]$ as defined in Reference [7] and [11]. The two figures show that the TD structure and the displacement field during the CTB migration will depend on the applied stress. Please note there must be two values of the horizontal displacement because the two neighboring Mg atoms at CTB are not equivalent from the perspective of crystallography. This is considered to be the structural origin of why twinning cannot be achieved by homogeneous shear, and atoms must shuffle [35].

In Fig. 7, the structural variation of the CTB under the stress field is revealed. However, it is the potential energy at a few key configurations, including: (1) the starting configuration, (2) the configuration of the saddle point (usually the one where TDs nucleate), and (3) the final configuration, which determines the energy barrier physically. It is

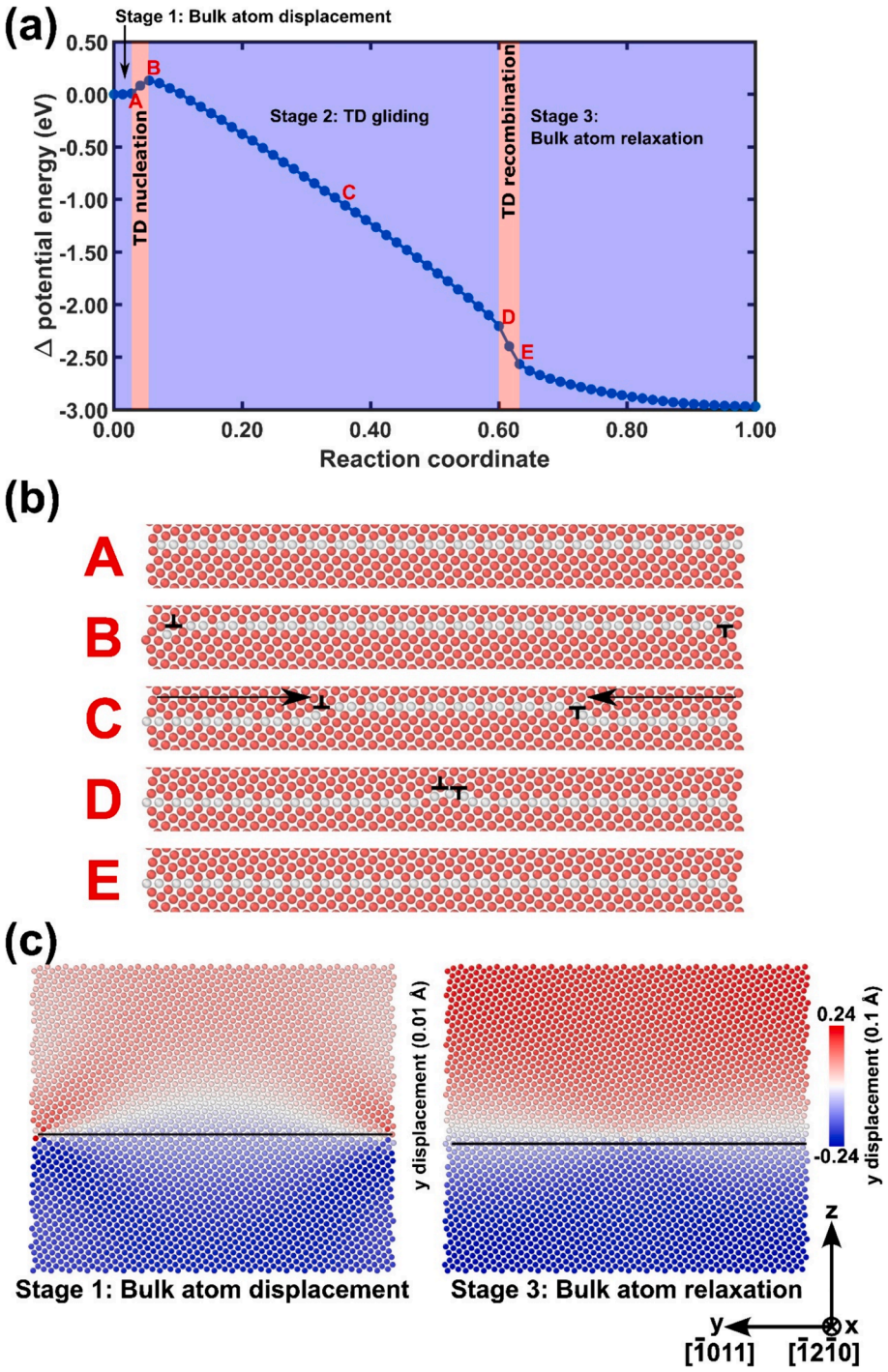

Fig. 6. (a) The minimum energy path (MEP) of the coherent twin boundary migration under a shear stress of 0.5 GPa. Stage 1 (bulk atom displacement), TD nucleation, Stage 2 (TD gliding), TD recombination and Stage 3 (bulk atom relaxation) are colored along the MEP. Five representative states (replicas) A-E are labeled, and their atomic configurations are presented in (b). Atoms are colored based on their local structural environment, red: hcp, gray: boundary atoms that are not of any specified crystal structure type. (c) The atomic displacement during Stage 1 and Stage 3 along the y direction. Note that the unit of y displacement is 0.01 Å and 0.1 Å for the left figure in (c) and the right figure in (c), respectively.

found that the correlation between structure and energy is not realized when checking the structural unit at the three key configurations. For example, a larger relative horizontal displacement (i.e., the y value in Fig. 7(f) and 7(g)) does not necessarily result in a higher energy barrier.

Fig. 8(a)–(d) show the relative horizontal displacement normalized by the length of $[10\bar{1}1]$ for atoms in the initial CTB, denoted as α, under four loading conditions. At the position of TDs, which is denoted by the red- and magenta-colored dots, again, α will have the same meaning as its Burgers vector of a TD normalized by $[10\bar{1}1]$ as discussed in [7]. The contour represents the relative atomic horizontal displacement value at the specific replica (x-direction) and for the specific atom (y-direction). The behavior for a total of 40 atoms at the initial CTB is shown. The atomic numbering and how the relative horizontal displacement of CTB atoms is calculated are the same as illustrated in Fig. 7(a) and (b). The left white line labels the TD nucleation, while the right one is for the TD recombination. Contours in Fig. 8(a)-(d) are mostly serrated because of

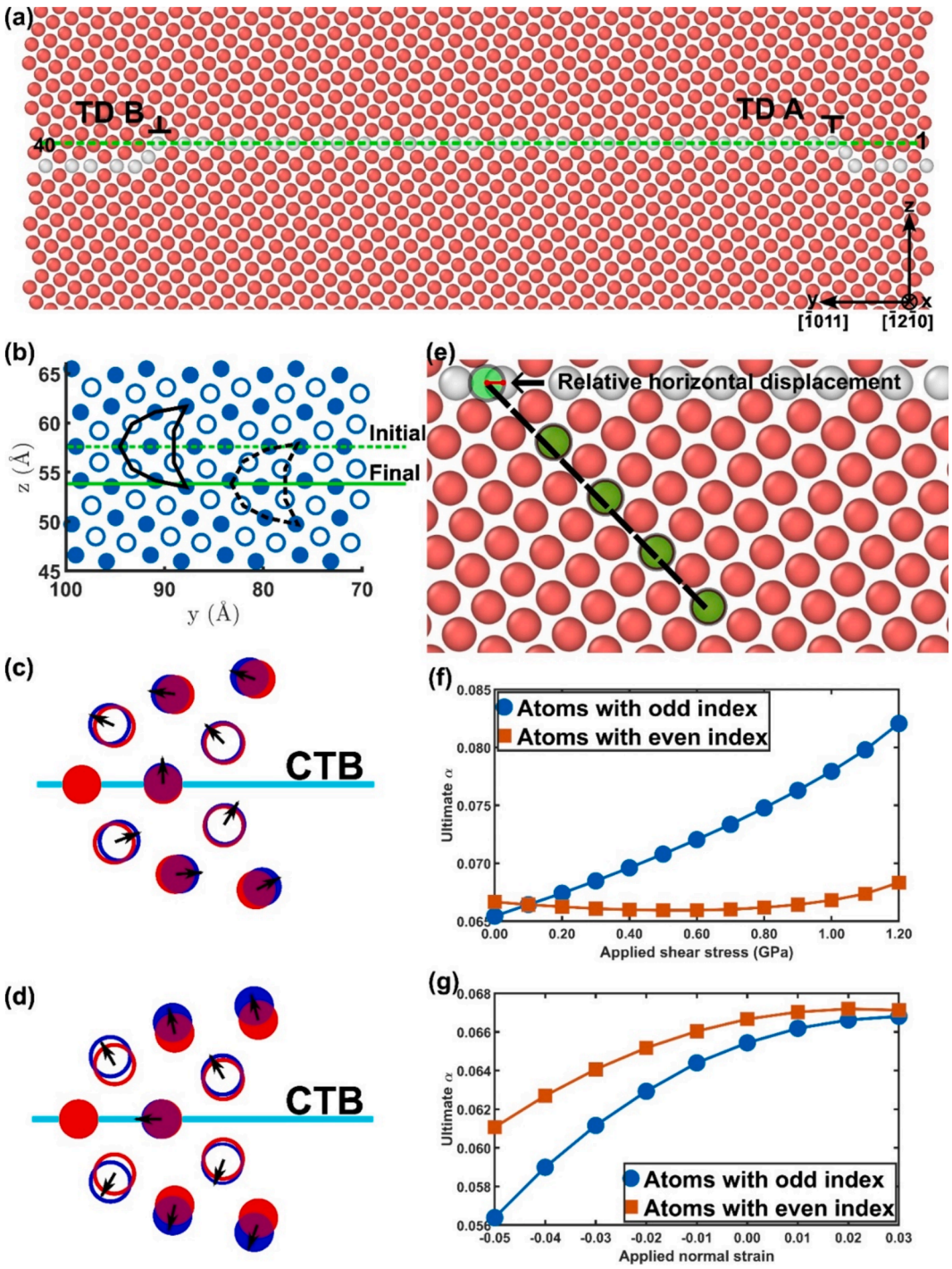

Fig. 7. (a) Diagram showing a typical configuration during the coherent twin boundary (CTB) migration in which the atom number and twinning disconnection A and B in (c)-(f) are defined. (b) Kite-shaped structural unit of atoms (outlined in black) in the vicinity of the initial CTB and the final CTB under the stress-free condition. The atoms represented by the filled circles have a different x coordinate than those represented by the open circles. (c) The evolution of one representative structural unit under increasing shear stress from 0 (the red atoms) to 1.2 GPa (the blue atoms); (d) The evolution of one representative structural unit when the normal strain goes from 5 % compressive (the red atoms) to 3 % tensile (the blue atoms). (e) Diagram showing the CTB and its vicinity in which relative horizontal displacement of CTB atoms is defined. The displacement is exaggerated for illustrative purposes. (f) The necessary relative horizontal displacement for atoms in the initial CTB to move to their final positions, normalized by the length of $[10\bar{1}1]$ (denoted as ultimate α) as a function of shear stress; (g) Ultimate α for atoms in the initial CTB as a function of normal strain.

the nonequivalence of two neighboring Mg atoms at the CTB.

It is worth noting that the atomic displacement keeps increasing during the whole migration process. In other words, the reorientation of crystal from matrix to twin is not fully completed right after a TD passes or after TDs annihilate. It is only true that atomic displacement increases at the largest rate as a TD passes that atom. The relative displacement is unable to reach the ideal value at a fully relaxed TD, about $\frac{1}{15}[10\bar{1}1]$, which is given by [7]:

$$b_{tw} = \lambda[10\bar{1}1],\ \lambda = \frac{3-\kappa^2}{3+\kappa^2} \tag{6}$$

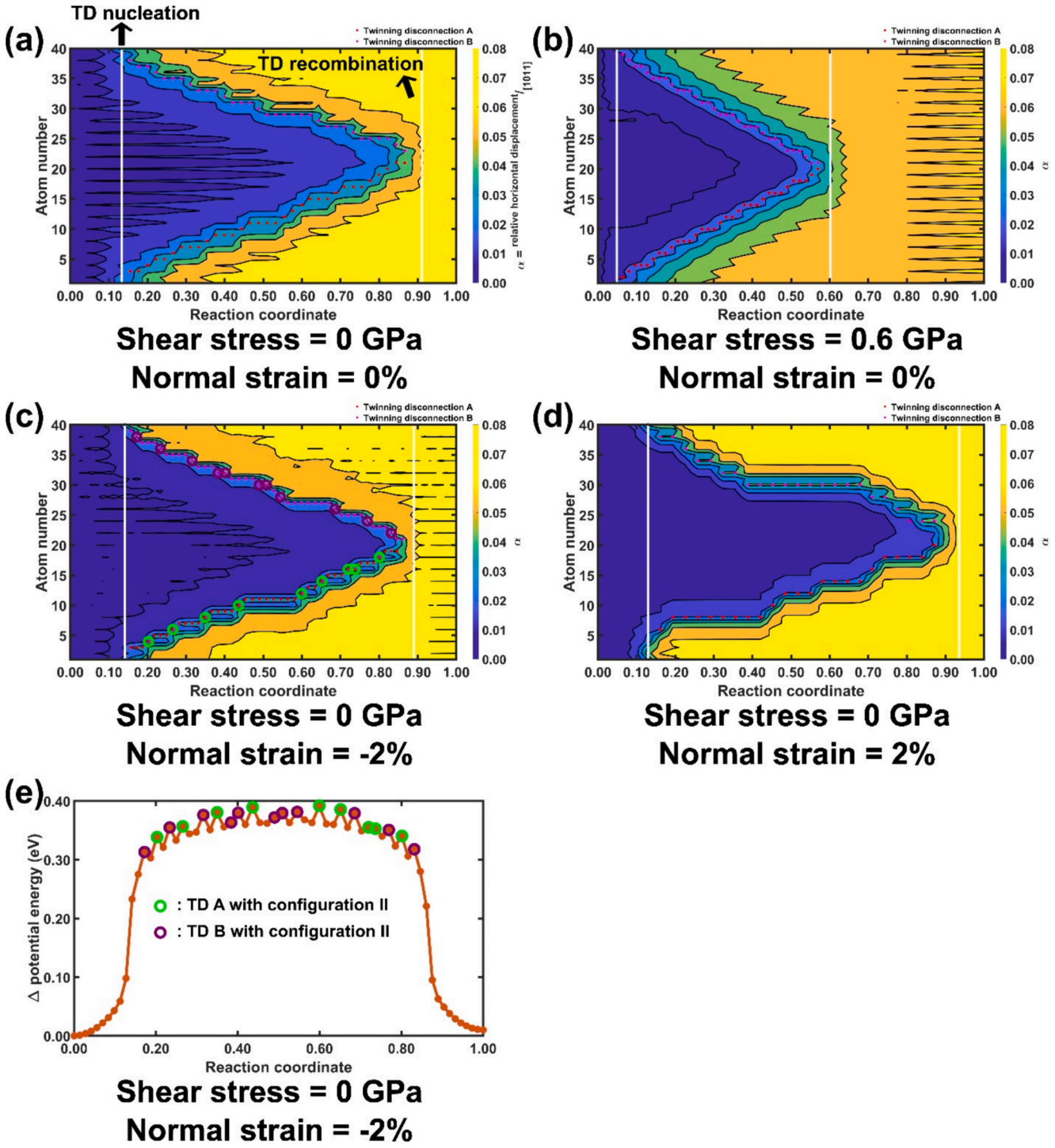

Fig. 8. The contour plots show the relative horizontal atomic displacement normalized by the length of $[10\bar{1}1]$ (denoted as α) of 40 atoms in the initial coherent twin boundary by each replica under (a) stress free condition (no imposed shear stress and normal strain); (b) pure shear stress of 0.6 GPa; (c) a compressive strain of 2%; and (d) a tensile strain of 2%. In all the contour plots, the red and magenta dots represent the position of two twinning disconnections (TDs), while the left white line means the replica where TDs nucleate and the right one means the replica where TDs recombine. Specifically, in (c), a few TDs A and TDs B with the non-dominant TD configuration are highlighted in green and purple circles and correspond to the replicas labeled in the same way in (e), the minimum energy path under a compressive strain of 2%.

where κ is c/a in Mg, until the final configuration of the stress-free migration. We find that the relative atomic displacement at TDs in the intermediate states are smaller than the above theoretical value and no longer a constant.

Consistent with the migration mechanism, there is no systematic variation of the relative displacement but only some value changes caused by different loading conditions, as shown by Fig. 8(a)–(d).

The discrepancy of the relative atomic displacement at TDs may be caused by the arrangement of the initial and final configuration. When the initial and final configurations are strictly fixed with boundary conditions along x and y being PBCs, it seems that the MEP will favor a steady reorientation instead of an abrupt one that completes as soon as

TD sweeps through. This is also why bulk atoms would move before TD nucleation and after TD recombination. It should be noted that the TD configurations observed in this study are not energetically stable because the intermediate state is not at a local minimum. Therefore, they cannot be present for a long period and may evolve to the commonly reported TD configuration with an atomic displacement of $\boldsymbol{b}_{tw}$ in a fully relaxed system. However, interestingly, NEB predicts that the steady reorientation assisted by the energetically unstable TD could lower the energy barrier more so than the commonly reported TD. While this result needs verification it nonetheless opens the possibility of a non-conventional TD configuration during CTB migration.

4.3. Two different configurations of twinning disconnections (TDs)

From the above discussion, TDs are key to understanding CTB migration because: (1) TD nucleation consumes the most energy, and the replica where the pair of TDs nucleates sits at the saddle point for cases in the large shear stress regime; (2) the TD is the only defect other than twin boundary during the CTB migration process.

The core structure of TDs can be represented by the atomic configuration near the TDs (i.e., relative positions of atoms). Fig. 9 shows two different configurations of the TDs observed along the MEPs. Although they both have two atomic layer-high steps and similar relative atomic displacement at TDs, the atomic configuration of the step can be classified into two categories in Fig. 9(a) and 9(b), denoted as configuration I and configuration II. Atoms are colored according to their local structural environment using the polyhedral template matching method in OVITO [36]. The red atoms have a hcp-type environment while the gray atoms are the boundary atoms which have no specified structure type. Following the pattern of the gray atoms, there are two atomic layers highlighted by green lines, which are nearly flat (i.e., all atoms in the atomic layer are with nearly the same z coordinate) and represent the two twin boundaries and have a TD between them. The structural reason for these two different TD configurations is that the two nearest-neighboring Mg atoms at CTB are not equivalent, and the step can be at either of them.

The parity of atom number of the red and magenta dots in Fig. 8(a)-(d), which means the position of the dislocation core of the TD, indicate which TD configuration is at the specific replica – whether the TD is at the atom with an odd or even index indicates which TD configuration it is. Energetically, the two TD configurations are different, and each would be preferred under different stress fields. While there is no stress applied to the system, Fig. 8(a) shows it is possible to observe both of these two configurations during the migration process. Under a compressive strain, Fig. 8(c) shows configuration A is dominant, while under a tensile strain, Fig. 8(d) shows configuration B is preferred.

It is shown in Fig. 2(a) that the MEP curve of 2 % compressive strain appears to fluctuate, especially at the stage of TD gliding. The fluctuation results from the switch between the two TD configurations and indicates the potential energy difference between the two configurations. Fig. 8(e) simply takes the MEP curve of 2 % compressive strain with labels as an example. The highlighted points in Fig. 8(e) are replicas with local potential energy maximum. They correspond to the circles with the same color in Fig. 8(e) and are the replicas where one of TDs has a different configuration from the dominant configuration. The non-dominant TD configuration is of higher energy and thus is not energetically preferred under a certain loading. A similar fluctuation in the MEP is also seen but with lower amplitude when there is no normal strain, indicating the two configurations may be of a comparable energy value when the normal strain approaches 0. On the contrary, there is no such fluctuation in the MEP curve if the normal strain turns 2 % tensile, because configuration B with lower energy is observed at almost all the replicas during the stage of TD gliding. Apparently, the potential energy difference between the two TD configurations is larger when the compressive strain or the tensile strain increases. From those cases varying the shear stress, it appears that the shear stress would not result in any significant preference on the two configurations.

5. Conclusions

This NEB-based study reveals a systematic stress-dependent energy barrier calculation for CTB migration. We find that while applying a shear stress lowers the energy barrier and boosts CTB migration, a non-glide stress changes the energy barrier. When the shear stress is non-zero, thereby inducing an asymmetry in the MEP and driving CTB migration, a compressive stress can reduce the energy barrier and the CRSS, and a tensile stress can increase it. Assuming the Arrhenius equation applies, the rate of CTB migration is shown to be proportional to the ratio between the TRSS and the non-glide stress dependent CRSS to the power of a constant under a given temperature. We note that the model considering the impact of the non-glide stress can be used to predict the twinning behavior under a complex stress field.

In addition to the energy barrier, the migration mechanism is also revealed by the structural evolution during CTB migration, especially that of TDs. While the migration mechanism does not change with the imposed stress, the dominant TD configuration may be different upon either tensile or compressive stress because one of the two possible TD configurations is more energetically favorable. On the other hand, the TD configuration itself in the intermediate state does not match with the widely reported TD configuration for a $\{10\bar{1}2\}$ twin boundary and has a smaller and non-constant relative atomic displacement at the TD at every applied stress, which shows that the local reorientation during the CTB migration process does not complete as the TD passes through. Other than the behavior of TDs, the bulk atom displacement/relaxation before TD nucleation and after TD recombination is also important to activate/conclude the CTB migration. These findings complement the current understanding of twin boundary migration. Future studies will focus on migration of the incoherent twin boundary and twin boundary

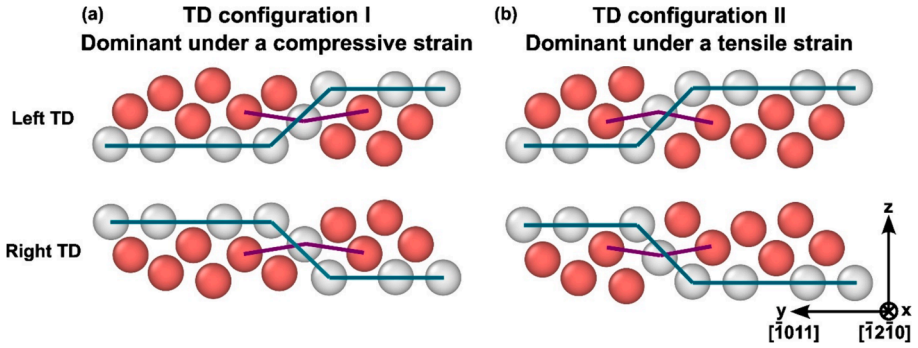

Fig. 9. Two prevalent twinning disconnection configurations under (a) compressive strain and (b) tensile strain. Atoms are colored based on their local structural environment. Green and purple lines are added as a guide to the eyes to show the difference between the two configurations.

with segregation where interactions between TD and other defects are possible.

CRediT authorship contribution statement

Kehang Yu: Writing – review & editing, Writing – original draft, Visualization, Methodology, Investigation, Formal analysis, Data curation, Conceptualization. **Xin Wang:** Writing – review & editing, Conceptualization. **Subhash Mahajan:** Writing – review & editing, Supervision, Funding acquisition, Conceptualization. **Timothy J. Rupert:** Writing – review & editing, Supervision, Resources, Funding acquisition, Formal analysis, Conceptualization. **Irene J. Beyerlein:** Writing – review & editing, Supervision, Funding acquisition, Formal analysis, Conceptualization. **Penghui Cao:** Writing – review & editing, Supervision, Methodology, Formal analysis, Conceptualization. **Julie M. Schoenung:** Writing – review & editing, Supervision, Project administration, Funding acquisition, Conceptualization. **Enrique J. Lavernia:** Writing – review & editing, Supervision, Project administration, Funding acquisition, Conceptualization.

Declaration of competing interest

The authors declare that they have no known competing financial interests or personal relationships that could have appeared to influence the work reported in this paper.

Data availability

Data will be made available on request.

Acknowledgements

The authors acknowledge financial support from the National Science Foundation (NSF CMMI-1729829, NSF CMMI-1729887 and NSF CMMI-1723539). This work utilized the infrastructure for high-performance and high-throughput computing, research data storage and analysis, and scientific software tool integration built, operated, and updated by the Research Cyberinfrastructure Center (RCIC) at the University of California, Irvine (UCI). The RCIC provides cluster-based systems, application software, and scalable storage to directly support the UCI research community.

References

[1] A. Imandoust, C.D. Barrett, T. Al-Samman, K.A. Inal, H. El Kadiri, A review on the effect of rare-earth elements on texture evolution during processing of magnesium alloys, J. Mater. Sci. 52 (2017) 1–29, https://doi.org/10.1007/s10853-016-0371-0.
[2] M.H. Yoo, Slip, twinning, and fracture in hexagonal close-packed metals, Metall. Trans. A 12 (1981) 409–418, https://doi.org/10.1007/BF02648537.
[3] D. Zhang, L. Jiang, B. Zheng, J.M. Schoenung, S. Mahajan, E.J. Lavernia, I.J. Beyerlein, J.M. Schoenung, E.J. Lavernia, Deformation Twinning (Update), in: Ref. Module Mater. Sci. Mater. Eng., Elsevier, 2016. doi: 10.1016/B978-0-12-803581-8.02878-2.
[4] I.J. Beyerlein, M. Arul Kumar, The Stochastic Nature of Deformation Twinning: Application to HCP Materials, in: W. Andreoni, S. Yip (Eds.), Handb. Mater. Model. Methods Theory Model, Springer International Publishing, Cham, 2018, pp. 1–39, https://doi.org/10.1007/978-3-319-42913-7_103-1.
[5] M.A. Kumar, I.J. Beyerlein, Local microstructure and micromechanical stress evolution during deformation twinning in hexagonal polycrystals, J. Mater. Res. 35 (2020) 217–241, https://doi.org/10.1557/jmr.2020.14.
[6] Y. Hu, V. Turlo, I.J. Beyerlein, S. Mahajan, E.J. Lavernia, J.M. Schoenung, T. J. Rupert, Embracing the chaos: alloying adds stochasticity to twin embryo growth, Phys. Rev. Lett. 125 (2020) 205503, https://doi.org/10.1103/PhysRevLett.125.205503.
[7] J. Wang, J.P. Hirth, C.N. Tomé, (-1012) Twinning nucleation mechanisms in hexagonal-close-packed crystals, Acta Mater. 57 (2009) 5521–5530, https://doi.org/10.1016/j.actamat.2009.07.047.
[8] J. Han, S.L. Thomas, D.J. Srolovitz, Grain-boundary kinetics: a unified approach, Prog. Mater. Sci. 98 (2018) 386–476, https://doi.org/10.1016/j.pmatsci.2018.05.004.
[9] A. Ostapovets, A. Serra, Review of non-classical features of deformation twinning in hcp metals and their description by disconnection mechanisms, Metals 10 (2020) 1134, https://doi.org/10.3390/met10091134.
[10] C.D. Barrett, H. El Kadiri, Impact of deformation faceting on 10–12}, {10-11 and 10–13 embryonic twin nucleation in hexagonal close-packed metals, Acta Mater. 70 (2014) 137–161, https://doi.org/10.1016/j.actamat.2014.02.018.
[11] A. Ostapovets, R. Gröger, Twinning disconnections and basal–prismatic twin boundary in magnesium, Model. Simul. Mater. Sci. Eng. 22 (2014) 025015, https://doi.org/10.1088/0965-0393/22/2/025015.
[12] L. Capolungo, I.J. Beyerlein, C.N. Tomé, Slip-assisted twin growth in hexagonal close-packed metals, Scr. Mater. 60 (2009) 32–35, https://doi.org/10.1016/j.scriptamat.2008.08.044.
[13] A. Serra, D.J. Bacon, A new model for 10–12 twin growth in hcp metals, Philos. Mag. A 73 (1996) 333–343, https://doi.org/10.1080/01418619608244386.
[14] A. Ishii, J. Li, S. Ogata, Shuffling-controlled versus strain-controlled deformation twinning: the case for HCP Mg twin nucleation, Int. J. Plast. 82 (2016) 32–43, https://doi.org/10.1016/j.ijplas.2016.01.019.
[15] O. MacKain, M. Cottura, D. Rodney, E. Clouet, Atomic-scale modeling of twinning disconnections in zirconium, Phys. Rev. B 10 (2017).
[16] L. Leclercq, L. Capolungo, D. Rodney, Atomic-Scale Comparison Between {1-101} and {1-102} Twin Growth Mechanisms in Magnesium, (2014) 9.
[17] X.-Z. Tang, Q. Zu, Y.-F. Guo, The diffusive character of extension twin boundary migration in magnesium, Materialia 2 (2018) 208–213, https://doi.org/10.1016/j.mtla.2018.07.017.
[18] Y. Sato, T. Swinburne, S. Ogata, D. Rodney, Anharmonic effect on the thermally activated migration of 10–12 twin interfaces in magnesium, Mater. Res. Lett. 9 (2021) 231–238, https://doi.org/10.1080/21663831.2021.1875079.
[19] N. Combe, F. Mompiou, M. Legros, Shear-coupled grain-boundary migration dependence on normal strain/stress, Phys. Rev. Mater. 1 (2017) 033605, https://doi.org/10.1103/PhysRevMaterials.1.033605.
[20] I.J. Beyerlein, L. Capolungo, P.E. Marshall, R.J. McCabe, C.N. Tomé, Statistical analyses of deformation twinning in magnesium, Philos. Mag. 90 (2010) 2161–2190, https://doi.org/10.1080/14786431003630835.
[21] A. Fernández, A. Jérusalem, I. Gutiérrez-Urrutia, M.T. Pérez-Prado, Three-dimensional investigation of grain boundary–twin interactions in a Mg AZ31 alloy by electron backscatter diffraction and continuum modeling, Acta Mater. 61 (2013) 7679–7692, https://doi.org/10.1016/j.actamat.2013.09.005.
[22] M.R. Barnett, Z. Keshavarz, A.G. Beer, X. Ma, Non-Schmid behaviour during secondary twinning in a polycrystalline magnesium alloy, Acta Mater. 56 (2008) 5–15, https://doi.org/10.1016/j.actamat.2007.08.034.
[23] C. Lou, X. Zhang, Y. Ren, Non-schmid-based 10–12 twinning behavior in polycrystalline magnesium alloy, Mater. Charact. 107 (2015) 249–254, https://doi.org/10.1016/j.matchar.2015.07.022.
[24] S. Xu, L.S. Toth, C. Schuman, J.-S. Lecomte, M.R. Barnett, Dislocation mediated variant selection for secondary twinning in compression of pure titanium, Acta Mater. 124 (2017) 59–70, https://doi.org/10.1016/j.actamat.2016.10.063.
[25] L. Capolungo, P.E. Marshall, R.J. McCabe, I.J. Beyerlein, C.N. Tomé, Nucleation and growth of twins in Zr: A statistical study, Acta Mater. 57 (2009) 6047–6056, https://doi.org/10.1016/j.actamat.2009.08.030.
[26] Q. Qin, J.L. Bassani, Non-schmid yield behavior in single crystals, J. Mech. Phys. Solids 40 (1992) 813–833, https://doi.org/10.1016/0022-5096(92)90005-M.
[27] I.J. Beyerlein, C.N. Tomé, A probabilistic twin nucleation model for HCP polycrystalline metals, Proc. r. Soc. Math. Phys. Eng. Sci. 466 (2010) 2517–2544, https://doi.org/10.1098/rspa.2009.0661.
[28] R.A. Lebensohn, C.N. Tomé, A study of the stress state associated with twin nucleation and propagation in anisotropic materials, Philos. Mag. A 67 (1993) 187–206, https://doi.org/10.1080/01418619308207151.
[29] C.D. Barrett, H. El Kadiri, M.A. Tschopp, Breakdown of the Schmid law in homogeneous and heterogeneous nucleation events of slip and twinning in magnesium, J. Mech. Phys. Solids 60 (2012) 2084–2099, https://doi.org/10.1016/j.jmps.2012.06.015.
[30] K. Ito, V. Vitek, Atomistic study of non-Schmid effects in the plastic yielding of bcc metals, Philos. Mag. A 81 (2001) 1387–1407, https://doi.org/10.1080/01418610108214447.
[31] S. Plimpton, Fast parallel algorithms for short-range molecular dynamics, J. Comput. Phys. 117 (1995) 1–19, https://doi.org/10.1006/jcph.1995.1039.
[32] Z. Wu, M.F. Francis, W.A. Curtin, Magnesium interatomic potential for simulating plasticity and fracture phenomena, Model. Simul. Mater. Sci. Eng. 23 (2014) 015004, https://doi.org/10.1088/0965-0393/23/1/015004.
[33] A. Stukowski, Visualization and analysis of atomistic simulation data with OVITO–the Open Visualization Tool, Model. Simul. Mater. Sci. Eng. 18 (2010) 015012, https://doi.org/10.1088/0965-0393/18/1/015012.
[34] G. Henkelman, B.P. Uberuaga, H. Jónsson, A climbing image nudged elastic band method for finding saddle points and minimum energy paths, J. Chem. Phys. 113 (2000) 9901–9904, https://doi.org/10.1063/1.1329672.
[35] J.W. Christian, S. Mahajan, Deformation twinning, Prog. Mater. Sci. 39 (1995) 1–157, https://doi.org/10.1016/0079-6425(94)00007-7.
[36] P.M. Larsen, S. Schmidt, J. Schiøtz, Robust structural identification via polyhedral template matching, Model. Simul. Mater. Sci. Eng. 24 (2016) 055007, https://doi.org/10.1088/0965-0393/24/5/055007.